The Astronomical Journal, 139:2600–2611, 2010 June doi:10.1088/0004-6256/139/6/2600

A ∼ 40 YEAR VARIABILITY CYCLE IN THE LUMINOUS BLUE VARIABLE/WOLF–RAYET BINARY SYSTEM HD 5980?

Gloria Koenigsberger[1], Leonid Georgiev[2], D. John Hillier[3], Nidia Morrell[4], Rodolfo Barbá[5,6], and Roberto Gamen[7]
[1] Instituto de Ciencias Físicas, Universidad Nacional Autónoma de México, Av. Universidad s/n, Cuernavaca, Mor. 62210, Mexico; gloria@astro.unam.mx
[2] Instituto de Astronomía, Universidad Nacional Autónoma de México, Apartado Postal 70-264, México D.F. 04510, Mexico; georgiev@astro.unam.mx
[3] Department of Astronomy, 3941 O'Hara Street, University of Pittsburgh, Pittsburgh, PA 15260, USA; djh@rosella.phyast.pitt.edu
[4] Las Campanas Observatory, The Carnegie Observatories, Colina El Pino s/n, Casillas 601, La Serena, Chile; nmorrell@lco.cl
[5] Departamento de Física, Universidad de la Serena, Benavente 980, La Serena, Chile; rbarba@dfuls.cl
[6] ICATE-CONICET, San Juan, Argentina
[7] Facultad de Ciencias Astronómicas y Geofísicas, Universidad Nacional de La Plata, and Instituto de Astrofísica de La Plata (CCT La Plata-CONICET), Paseo del Bosque S/N, B1900FWA, La Plata, Argentina; rgamen@gmail.com
Received 2010 February 4; accepted 2010 April 17; published 2010 May 10

ABSTRACT

The massive Wolf–Rayet stellar system HD 5980 in the Small Magellanic Cloud entered a sudden and brief ∼ 1–3 mag eruptive state in the mid-1990s. The cause of the instability is not yet understood, but mechanisms similar to those in luminous blue variables are suspected. Using a previously unreported set of spectroscopic data obtained in 1955–1967 and recently acquired optical and *HST*/STIS spectra, we find that (1) the brief eruptions of 1993 and 1994 occurred at the beginning of an extended (∼ decades) high state of activity characterized by large emission-line intensities; (2) the level of activity is currently subsiding; and (3) another strong emission-line episode appears to have occurred between 1960 and 1965, suggesting the possibility that the long-term cyclical variability may be recurrent on a ∼ 40 year timescale. These characteristics suggest the possible classification of HD 5980 as an S Doradus-type variable. The effects due to binary interactions in the system are discussed, and we tentatively suggest that the short duration and relatively hot spectral type (WN11/B1.5I) observed during maximum in the visual light curve may be attributed to these interactions.

Key words: binaries: eclipsing – stars: individual (HD 5980) – stars: variables: S Doradus – stars: Wolf–Rayet

Online-only material: color figures

1. INTRODUCTION

HD 5980 is an eclipsing and eccentric binary system in the Small Magellanic Cloud that presented a luminous blue variable (LBV)-like eruptive state between 1993 and 1994 (Bateson & Jones 1994; Barbá et al. 1995; Koenigsberger et al. 1995). Its spectrum discloses the presence of three luminous objects: two emission-line stars that are in a close 19.3 day binary orbit (Breysacher & Perrier 1980) and a third O-type object whose photospheric absorptions remain relatively stationary on these orbital timescales (Niemela 1988; Koenigsberger et al. 2002). Following the convention introduced by Barbá et al. (1996), we label as Star A the star "in front" at an orbital phase $\phi = 0.00$ and Star B the one "in front" at $\phi = 0.36$, the opposite eclipse. Star C is the third component. Despite the eclipsing nature of the close binary, the masses are very uncertain because their determination hinges on how one interprets the radial velocities (RVs) of the emission lines and on the specific lines that are used. The current estimates suggest $M_A \sim 50$–$79\ M_\odot$ and $M_B \sim 28$–$67\ M_\odot$ (Niemela 1988; Foellmi et al. 2008). Star A is the component whose spectral type has changed from the hot Wolf–Rayet subtype WN3 through subsequently cooler nitrogen subtypes culminating in WN11 during the 1994 eruptive phase (Niemela 1988; Barbá et al. 1996; Drissen et al. 2001; Heydari-Malayeri et al. 1997). Star B is believed to be a WN4 star (Breysacher et al. 1982; Niemela 1988). Its derived radius (∼16 $R_\odot$; Perrier et al. 2009) and mass are significantly in excess of values associated with Galactic WNE stars by Hamann et al. (1993), which could be explained if it contains hydrogen and, since the lower metallicity of the SMC leads to a systematic shift in spectral types to earlier types (Crowther 2006), it is possible that star B's intrinsic properties correspond more to those of Galactic WN6–WN7 stars. Furthermore, there is evidence suggesting that it is also a variable (Villar-Sbaffi et al. 2003).

Breysacher & Perrier (1991) and Perrier et al. (2009) derived the relative luminosities of the three objects. Their approach considers the presence of an extended envelope only around star B. Although it could be argued that neglect of the extended envelope of star A limits the results of their analysis, it turns out that their data were acquired when star A was relatively inactive (Section 3), and thus it is a relatively good approximation for the data that they analyzed. Adopting the masses estimated by Foellmi et al. (2008), they find that the eclipsing stars have radii $R_A = 22.7$–25.1 and $R_B = 15.6$–$17.2\ R_\odot$. The system's parameters, as they are currently understood, are summarized in Table 1. For further background on HD 5980's observational characteristics up to the year 2000 and a description of early studies of its properties see Moffat et al. (1998), Koenigsberger (2004), and Barbá et al. (1996, 1997) for a description of the spectrum at epochs before, during, and after the eruptive event.

Gaining an understanding of the intriguing properties of HD 5980 is important for many reasons. It is associated with a young and massive stellar cluster in a low-metallicity region typical of distant galaxies. Thus, its behavior provides important clues for understanding evolutionary processes in dense star-forming regions that lie at cosmological distances. It also provides an excellent laboratory for studying binary interaction effects as well as the mass-loss that shapes the pre-supernova circumstellar environment. Hence, it is important to determine the underlying characteristics of the stars that make up the system and their evolutionary state. In this paper, we focus

Table 1
Summary of HD 5980 Estimated Parameters

Parameter	Values	Epoch	References
$P_{\rm orb}$	19.2654 d		Sterken & Breysacher 1997
i	88°		Moffat et al. 1998
a	127 $R_\odot$		Niemela et al. 1997
	143–157 $R_\odot$		Foellmi et al. 2008
e	0.30±0.16		Foellmi et al. 2008
$M_{\rm A}$	50 $M_\odot$		Niemela et al. 1997
	58–79 $M_\odot$		Foellmi et al. 2008
$M_{\rm B}$	28 $M_\odot$		Niemela et al. 1997
	51–67 $M_\odot$		Foellmi et al. 2008
l_A	0.398 ± 0.021	1978	Perrier et al. 2009
l_B	0.300 ± 0.016	1978	Perrier et a. 2009
$R_{\rm A}$	23–25 $R_\odot$	1978	Perrier et al. 2009
	280 $R_\odot$	1994 Sep	Drissen et al. 2001
	150 $R_\odot$	1994 Dec	Koenigsberger et al. 1998a
$R_{\rm B}$	16–17 $R_\odot$		Perrier et al. 2009
$R_{\rm envB}$	39–43 $R_\odot$		Perrier et al. 2009
N[He]/N[H]$_{\rm Non\text{-}LTE}$	0.4	1994 Dec 30	Koenigsberger et al. 1998b
$\dot{M}_A$	10^{-3} $M_\odot$ yr^{-1}	1994 Dec 30	Koenigsberger et al. 1998b
L_A	3×10^6 $L_\odot$	1994 Dec 30	Koenigsberger et al. 1998b
	10^7 $L_\odot$	1994 Sep	Drissen et al. 2001
T_*^A	21,000 K	1994 Nov 24	Koenigsberger et al. 1996
	35,500 K	1994 Dec 30	Koenigsberger et al. 1998b
$V_{\rm rot}^A \sin i$	250 km s^{-1}		Georgiev & Koenigsberger 2004
$V_{\rm rot}^C \sin i$	75 km s^{-1}		Koenigsberger et al. 2001
$P_{\rm orb}$(C)	96.5 d		Schweickhardt 2000

our attention on its long-term spectroscopic characteristics. For this, we use recently acquired *Hubble Space Telescope* (*HST*) observations and ground-based data, and previously unreported optical-wavelength spectra that were collected between 1955 and 1960 ("historic" data), together with archival *International Ultraviolet Explorer* (*IUE*), *HST*, and FEROS data covering the years 1978–2006. This paper is organized as follows. The historic and new observational data are presented in Section 2; in Section 3, we focus on the long-term behavior; the variability on orbital timescales is discussed in Section 4; and Section 5 contains the conclusions.

2. OBSERVATIONAL DATA

2.1. New Observations

HD5980 was observed under *HST* Cycle 17 Program 11623 on 2009 September 9, using the newly serviced Space Telescope Imaging Spectrograph on board the *Hubble Space Telescope* (*HST*/STIS). The orbital phase at mid-exposure of the high-dispersion spectrum is 0.992, according to the Sterken & Breysacher (1997) ephemeris.[8]

The MAMA detector was used with the E140M grating obtaining a resolution ∼0.02 Å in the λλ1150–1720 wavelength range (∼4 km s^{-1} at 1400 Å; Kimble et al. 1998). The exposure was split into two segments of 2548 and 2627 s, respectively. The combined spectrum has signal-to-noise ratio, S/N ∼ 40 at 1280 Å and ∼ 20 at 1680 Å. The spectrum was processed through the standard STScI pipeline.

An intermediate resolution optical spectrum of HD5980 was obtained on 2009 August 29, using the Magellan I 6.5 m (Baade) telescope at Las Campanas Observatory, plus the Inamori Magellan Areal Camera and Spectrograph (IMACS) in its long camera (f/4) mode. We used a 600 line mm^{-1} grating and a 0.″9 long slit, providing wavelength coverage from 3700 Å to 6800 Å at a reciprocal dispersion of 0.37 Å pixel^{-1} and a spectral resolution of 1.4 Å as measured from the FWHM of the lines in the comparison lamp spectrum. The total exposure time was 400 s, split into two individual exposures, achieving an S/N which ranges from 200 to 300. A He–Ne–Ar spectrum was acquired immediately after the star observation, in order to derive wavelength calibration. Two flux standards (LTT7379 and LTT7987) were also observed during the night. The normal series of dome flats and bias were also secured. Reductions were carried out using standard IRAF[9] routines. The spectrum falls along chips 1–4 from the IMACS 8 chips array; leaving three narrow gaps of approximately 20 Å each between chips, namely at 4427–4445, 5217–5237, and 6019–6037 Å, respectively.

2.2. Historic and Archival Data

We obtained with the kind help of T. Lloyd Evans, M. Feast, and D. Kilkenny a collection of 22 photographic plates obtained in 1955–1962 with the two prism spectrographs attached to the Radcliffe telescope of the South African Astronomical Observatory. These spectra, having a dispersion of 89 Å mm^{-1} at Hγ, were digitized in the Bulgarian National Observatory "Rozhen" with the Joyce-Loebel densitometer, and the reductions were performed using the European Southern Observatory's (ESO's) MIDAS software.[10] For each spectrum, the photographic density was converted to intensity using the 12 calibration spots imprinted during the exposure on both sides of the spectrum. The photographic density was then first converted to Baker density (de Vaucouleurs 1968) and then a fifth-order polynomial

[8] Foellmi et al. (2008) find evidence suggesting that the initial epoch requires a small revision, but further analysis is required before adopting this suggested initial epoch.

[9] IRAF is distributed by the National Optical Astronomy Observatory, which is operated by the Association of Universities for Research in Astronomy, Inc., under cooperative agreement with the National Science Foundation.

[10] http://www.eso.org/sci/data-processing/software/esomidas/

was fitted to the resulting calibration curve. The dispersion of the points around the fit is smaller than the noise in the program star spectra, indicating that the error in the relative intensities for a given spectrum is dominated by the noise. Each density–intensity transformation was applied to all wavelengths of its corresponding spectrum. The wavelength calibration was performed using the two spectra of iron hollow cathode lamp generally imprinted above and below the program star spectrum. The formal error in the wavelength calibration is better than 18 km s^{-1}. After having performed the intensity and wavelength calibrations, each spectrum was normalized to the continuum obtained from a third- to fifth-order polynomial fit to its line free regions. The resulting spectra have S/N ∼ 10–15 between ∼ 4000 Å and the He II 4686 Å line, and drop rapidly to S/N ∼ 5 around Hβ+ He II. The S/N is also very poor near the blue end of the spectrum. The first two spectra of this collection were published by Feast et al. (1960).

Table 2 lists the ephemerides for the 22 Radcliffe spectra; the ESO/FEROS observations analyzed by Kaufer et al. (2002) and Foellmi et al. (2008); six additional ESO/FEROS spectra obtained in 2006 and processed in exactly the same manner as in Foellmi et al. (2008); and *HST*/STIS spectra analyzed by Koenigsberger et al. (2000); as well as the recent 2009 spectra. The table also contains data published by various authors. Column 1 lists a spectrum identifier; the year of observation is in Column 2; the modified Julian date (when available) is in Column 3; in Column 4, we list the corresponding orbital phase computed using $P = 19.2654$ and $T_0 = \mathrm{JD}2443158.7$ (Sterken & Breysacher 1997); and the last column indicates the origin of the data: R, Radcliffe (this paper); PM, P. Massey (1999, private communication); DM, Massey & Duffy (2001); H-M, Heydari-Malayeri et al. (1997); F, FEROS (Foellmi et al. 2008); H, *HST* (Koenigsberger et al. 2000); BW, Breysacher & Westerlund (1978); MT, Magellan Telescope (this paper).

2.3. Measurements of Emission-line Characteristics

In order to analyze the variability properties of HD 5980 over the ∼ 50 year baseline, we measured RVs, FWHM intensity, and equivalent widths (EWs) of the strongest lines present in the spectra. The line shapes in HD 5980 are significantly asymmetric and the degree and type of asymmetry change over the orbital cycle. Therefore, most standard theoretical line profiles are generally poor approximations to the actual line shape. However, it is not clear what alternative method might be more useful since the source of the asymmetries and variability is not yet established. We thus opted for the use of Gaussian fits as the most straightforward and objective measure of the RV, FWHM, and EW parameters, for the purpose of analyzing their temporal variability. We stress, however, that these RVs have little physical meaning generally and cannot be used as a representative of orbital motion. For the EWs, the Gaussian fits yield values that differ by ∼7% from values obtained by direct integration over the line profile, for a fixed value of the continuum level. This is smaller than the uncertainty that stems from the uncertainty in the choice of the continuum level.

The choice of the continuum level is dictated by the portions of the spectral energy distribution that are assumed to be free of lines. In the case of He II 4686, the neighboring spectral region contains the blend of N V and N III lines on the blue side and He I 4713 on the red side, the strength of which depends on whether the spectrum of HD5980 is WNE (pre-1990s) or WNL. Similarly, Hβ+ He II's neighboring continuum includes varying degrees of contamination by He I 4921. We estimate that the uncertainty due to the choice of the continuum is in general ∼ 15% except for the Hβ+ He II values in the Radcliffe data, where the average uncertainty is ±40% because this line lies near the edge of the photographic plate. Note, however, that once a specific criterion for the definition of the neighboring continuum level has been established, the EW measurements can be repeated consistently within ∼ 3% on spectra obtained with the same instrument and same epoch. Thus, the orbital-phase-dependent variability can generally be measured with this uncertainty, within a given data set. Measurements of the integrated fluxes in emission lines observed in the 1999, 2000 *HST*/STIS observations are listed in Table 3.

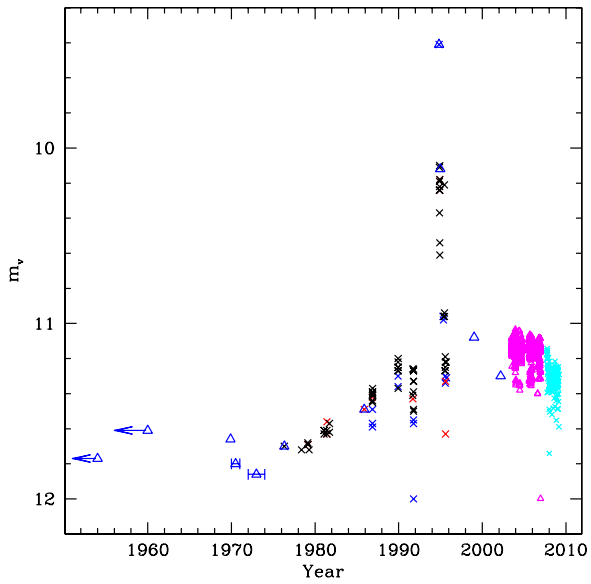

Figure 1. Visual magnitude measurements of HD 5980 from the *IUE* FES counts (black crosses); sources from the literature listed in the text (open triangles); and data from SWOPE and ASAS monitoring (small crosses). The arrows indicate that the date plotted for the observation (which corresponds to the date of publication of the paper in which the data are listed) is an upper limit. The large apparent scatter in data points of the same epoch is due largely to the eclipses.

(A color version of this figure is available in the online journal.)

Uncertainties in the RV and FWHM values are less sensitive to the choice of the continuum level. Using Gaussian fits to the line profiles, we find that the measurements can generally be repeated consistently within ±50 km s^{-1}, which we adopt for the uncertainty in these measurements. In the case of the Radcliffe data, the He II 4686 FWHM may be measured consistently within ±100 km s^{-1}, while average uncertainties in the Hβ+ He II FWHM measurements are ±200 km s^{-1}. Our measurements are listed in Columns 5–10 of Table 2.

3. LONG-TERM VARIABILITY

The light curve of HD 5980 covering the timespan 1950–2009 is illustrated in Figure 1, which contains visual magnitudes from Feast et al. (1960), Mendoza (1970), Azzopardi & Vigneau (1975), van den Bergh (1976), Koenigsberger et al. (1994), Massey & Duffy (2001), Foellmi et al. (2008), and from the All Sky Automated Survey (ASAS; Pojmanski 2002).

The slow brightening during the early 1980s can be unambiguously associated with the appearance of numerous emission lines at UV wavelengths such as N IV] 1486 Å as well as an increase in the strength of all the emissions (Koenigsberger et al. 1994, 1998a). Figure 2 illustrates the behavior of the energy flux contained in three UV lines over the timescale 1978–2009.

Table 2
He II 4686 and Hβ+ He II Measurements

Num	Year	MJD	ϕ	RV[a]	FWHM[a]	EW[b]	RV[a]	FWHM[a]	EW[b]	Notes
					He II 4686			Hβ+ He II		
2597	1955	35332.8	0.81	200	2290	35[c]	128	1754	7.7 [c]	R
2645	1955	35387.8	0.66	110	1802	98	16	1422	8.7	R
3074	1956	35741.8	0.04	294	1013	96	396	973	11.7	R
3793	1957	...	...	116	2070	73	265	1625	14	R
3872	1958	...	...	443	1217	79	283	1000	9.8	R
3882	1958	...	...	258:	1900:	63	258	1000	8.3	R
4613	1959	36915.8	0.98	181	1740	69	117	1740	18	R
4963	1960	...	...	174	1431	83	74	1227	10.7	R
5182	1961	37541.8	0.47	-99	1095	107	104	1300	13.5	R
5212	1961	37571.8	0.03	105	982	80	280	1000	15.3	R
5543	1962	...	...	429	1973	54	482	2115	12.2	R
5571	1962	...	...	388	1176	74	392	1249	14.4	R
5581	1962	37921.8	0.19	-220	2062	67	−124	2134	12.7	R
5586	1962	37924.8	0.35	210	1517	68	143	2000	14.0	R
5594	1962	...	0.6:	199	1511	71	110	1315	13.9	R
5601	1962	37932.8	0.77	189	1858	69	133	1731	18.1	R
5602	1962	37945.8	0.44	18	1300	77	32	1201	14.8	R
5603	1962	37953.8	0.86	1730	1880	82	...	...	13.2	R
5605	1962	...	0.98:	89	1754	72	230	1494	17.5	R
5611	1962	37958.8	0.12	225	1831	73	363	1690	12.4	R
6078	1963	...	...	13	1713	67	6	1455	11.6	R
7127	1965	...	...	200	2200	52	282	2390	11.0	R
...	1975	42684.1:	0.39	...	...	34.3	...	...	4.5	BW
...	1976	42973.1:	0.39	...	...	26.5	...	...	2.2	BW
...	1976	43083.1:	0.096	...	...	44	...	...	5.7	BW
...	1976	43084.1:	0.148	...	...	44.5	...	...	6.2	BW
...	1977	43194.1:	0.858	...	...	43.6	...	...	7.3	BW
...	81-84	...	...	...	...	82	...	...	...	PM
...	1989	47783.9	0.11	...	...	67	...	...	...	H-M
...	1991	48617.9	0.39	...	...	87	...	...	...	H-M
...	1993	⟨49259⟩	⟨0.36⟩	...	...	78	...	...	11.8	H-M
...	1994	⟨49605⟩	⟨0.73⟩	...	...	1.4	...	...	18.5	H-M
...	1994	49716.3	0.39	...	1400	81	...	900	47.5	K
03571	1998	51094.3	0.94	178	1527	76	243	1343	14.3	F
06981	1998	51100.3	0.24	334	1485	78	322	1212	14.1	F
08851	1998	51133.2	0.95	175	1477	66	146	1207	15.6	F
11811	1998	51138.0	0.20	316	1537	66	291	1167	14.9	F
14981	1998	51145.0	0.57	219	1251	88	152	1014	16.4	F
17081	1998	51150.0	0.83	205	1605	72	151	1368	16.1	F
23711	1998	51174.0	0.07	289	1066	71	252	920	15.0	F
24471	1998	51176.0	0.18	309	1500	72	282	1197	14.5	F
25781	1999	51181.0	0.44	154	927	67	126	733	13.0	F
26441	1999	51183.0	0.54	218	1143	83	154	909	16.4	F
27241	1999	51185.0	0.65	239	1360	92	168	1158	17.7	F
27941	1999	51187.0	0.75	225	1565	86	151	1286	17.7	F
28681	1999	51189.0	0.85	190	1617	68	166	1340	11.7	F
29441	1999	51191.0	0.95	204	1564	64	167	1211	11.3	F
30311	1999	51193.0	0.06	265	988	74	229	851	15.5	F
31461	1999	51197.0	0.27	315	1463	73	269	1021	15.2	F
o1020	1999	51304.8	0.83	367	1680	101	300	1500	25.4	H
o3020	1999	51308.4	0.05	430	1200	94	390	1080	19	H
o4020	1999	51310.3	0.15	440	1560	103	424	1440	24	H
o5020	1999	51314.4	0.36	357	1290	120	258	1135	20	H
o6020	1999	51315.3	0.40	358	1140	105	296	1055	18	H
79411	1999	51375.4	0.53	201	1173	102	152	1012	17.7	F
80871	1999	51379.4	0.73	216	1554	111	152	1356	18.1	F
82121	1999	51381.4	0.84	222	1552	96	161	1393	19.0	F
83811	1999	51383.4	0.94	221	1497	93	188	1334	17.6	F
84511	1999	51384.3	0.99	214	1382	105	188	1179	19.5	F
85181	1999	51385.3	0.04	278	1080	91	261	865	17.0	F
85771	1999	51386.4	0.10	306	1167	90	299	1090	17.8	F
86321	1999	51388.3	0.20	322	1490	92	341	1314	16.7	F
86701	1999	51389.4	0.25	323	1487	91	338	1168	14.9	F
87751	1999	51391.3	0.35	168	1281	119	136	1052	19.6	F
88931	1999	51392.3	0.40	151	1012	95	105	953	18.1	F

Table 2
(Continued)

Num	Year	MJD	ϕ	RV[a]	FWHM[a] He II 4686	EW[b]	RV[a]	FWHM[a] Hβ+ He II	EW[b]	Notes
90131	1999	51394.4	0.51	180	1100	102	139	997	17.6	F
...	2000	51830.	0.2	...	...	85	...	...	...	MD
o2020	2000	51654.6	0.01	385	1320	94	342	1074	18	H
0617801	2005	53538.4	0.80	217	1952	98	170	1792	17.2	F
0620221	2005	53541.4	0.96	251	1855	84	244	1590	13.4	F
0710740	2005	53561.4	0.99	239	1541	94	231	1215	15.8	F
0725630	2005	53576.3	0.77	269	1996	96	221	1803	15.8	F
0925220	2005	53638.2	0.98	235	1675	84	226	1346	13.6	F
0928161	2005	53641.2	0.13	340	1897	86	347	1716	14.4	F
1022731	2005	53665.0	0.37	136	1174	103	95	1150	16.7	F
f12	2006	53715.3	0.98	236	1661	84	224	1331	13.7	F
f34	2006	53716.0	0.02	255	1187	92	214	928	14.8	F
f56	2006	53731.0	0.80	218	1966	90	176	1858	15.0	F
f8	2006	53734.1	0.96	245	1902	73	266	1561	13.2	F
f9	2006	53735.0	0.01	243	1401	93	216	1160	16.9	F
f1112	2006	53738.0	0.16	334	1994	82	298	1738	13.0	F
BAA-1	2009	55073.4	0.45	122	1237	58	151	1320	8.7	M

Notes. Column 1 lists a spectrum identifier; the year of observation is in Column 2; the modified Julian date (when available) is in Column 3; in Column 4, we list the corresponding orbital phase computed using $P = 19.2654$ and $T_0 = \text{JD}2443158.7$ (Sterken & Breysacher 1997); and the last column indicates the origin of the data: R, Radcliffe (this paper); PM, P. Massey (1999, private communication); DM, Massey & Duffy (2001); H-M, Heydari-Malayeri et al. (1997); F, FEROS (Foellmi et al. 2008); H, *HST* (Koenigsberger et al. 2000); BW, Breysacher & Westerlund (1978); MT, Magellan Telescope (this paper).
[a] In units of km s^{-1}.
[b] In units of Å.
[c] The density-to-intensity calibration of this spectrum is uncertain.

Table 3
Integrated Fluxes from *HST*/STIS Observations

Year	MJD	ϕ	Flux (10^{-12} erg cm^{-2} –s)				
			He II 1640 (±0.5)	He II 1640 (±4)	He II 4686 (±0.1)	Hβ+ He II ±(0.2)	Hα (±1)
1999	51304.8	0.83	−4.8	140	5.1	3.6	21
1999	51308.4	0.05	−5.4	117	4.2	2.8	16
1999	51310.3	0.15	−3.5	131	5.3	3.4	20
1999	51314.4	0.36	−8.3	107	5.3	3.5	20
1999	51315.3	0.40	−8.0	110	5.3	3.1	20
2000	51654.6	0.01	−3.5	103	4.1	2.3	15

The N IV] 1486 and He II 1640 lines are particularly revealing. They show that the gradual intensity increase persisted beyond the time of the 1994 eruption. This is, indeed, similar to the m_v curve of Figure 1, which also suggests that the maximum in the gradual brightness trend was attained after the eruption maximum. Hence, we are led to conclude that the 1993–1994 eruptions simply interrupt momentarily the process by which the gradual line intensity and brightness growth are produced. This suggests that two distinct mechanisms are in action: the first produces a gradual and long-timescale effect, while the second (producing the sudden eruptions) acts on very short timescales once it is triggered.

Starting in 1999, a systematic decline in the m_v and line intensities is observed. The UV spectrum acquired during 2009 indicates that the spectral characteristics are reverting to those observed in spectra of the early 1980s. This raises the possibility that HD 5980's activity pattern may be cyclical. The data from the Radcliffe spectra suggest that, indeed, this may be the case. Figure 3 shows the long-term trends in the EW of He II 4686 and Hβ+ He II over the timescale 1955–2009. Although it is important to keep in mind the uncertainties inherent to line intensities derived from photographic plates, it is clear

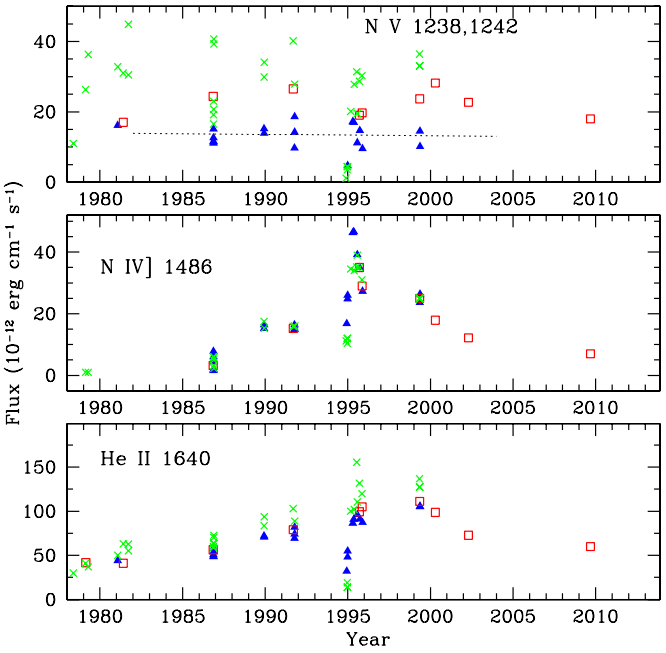

Figure 2. Long-term trend in the strength of UV emission lines. Different symbols correspond to orbital phase intervals as follows: star A "in back" (filled triangles)—$0.25 < \phi < 0.50$; star A "in front" (open squares) $-0.90 < \phi < 1.10$; other phases (crosses). The dotted line in the top panel is least-mean-squares fit to the $\phi \sim 0.36$ data and indicates constant flux values at this phase, within the uncertainties. Note that the maximum in line emission is attained after the 1994 eruptive event.

(A color version of this figure is available in the online journal.)

that line intensities around 1960 were stronger than during 1975–1982, indicating that during the latter years HD 5980 was at an activity minimum. This minimum is also present in the visual magnitudes. Hence, two maxima in the activity pattern

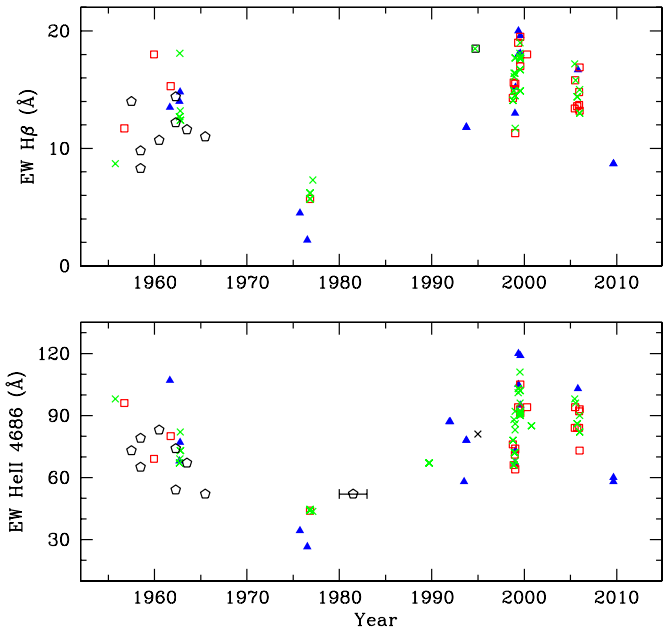

Figure 3. Long-term trend in the He II 4686 and Hβ+ He II EWs from the Radcliffe spectra and FEROS data. Different symbols correspond to orbital phase intervals as in the previous figure, but here we also include data for which no phase information is available (pentagons). Note that an earlier maximum appears to have occurred $\sim$ 1960, with a minimum between $\sim$ 1975 and 1980. (A color version of this figure is available in the online journal.)

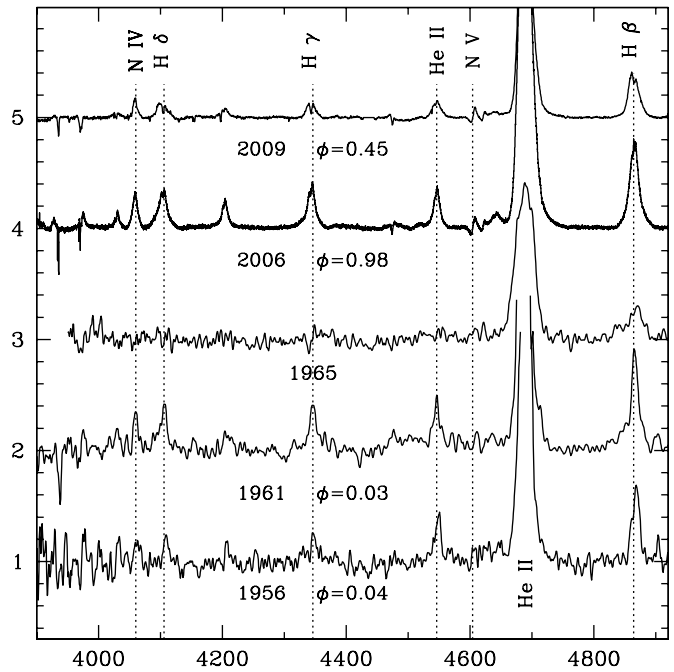

Figure 4. Montage of HD 5980 spectra between 1955 and 2009 showing that it is returning to a low activity state similar to that of 1965. The identification of the more prominent lines is listed. Note the weakening of all lines, and particularly the He II lines at 4200 and 4542 Å. Each spectrum is successively displaced vertically by 1 continuum unit for display purposes.

of HD 5980 seem to have occurred over a $\sim$ 40 year timescale suggesting that it may undergo recurring activity cycles over this timescale. If the current declining trend in the emission line intensities continues, a state of minimum similar to that of the late 1970s should be reached within the next few years.

There is no evidence for abrupt eruptions in the historic (1955–1965) data, although it may well be that due to its short duration, such an event might have gone undetected—the 1994 events might also have escaped detection had it not been for Albert Jones' systematic monitoring of the system, since there was no spectroscopic indication of the impending eruption just $\sim$ 50 days before the eruptive process started (Koenigsberger et al. 2006). It is also important to note that no large visual magnitude fluctuations appear to be present in the 425 Harvard Patrol Plates covering epochs between 1899 and 1951 (M. Hazen 2005, private communication), although they do indicate that $m_v \sim 11.4$ until around the year 1918, when a slow decline to $m_v \sim 11.8$ occurred. Between 1936 and 1951 it remained at this low state, but with several brief brightness enhancements.

Shown in Figure 4 is a selection of spectra from 1956 to 2006 along with the latest spectrum acquired in 2009 August. The latter shows significantly weaker emission lines, and the He II 4686 and Hβ+ He II EWs are close to those reported in the mid-1970s. Hence, there is little question that the current activity cycle is approaching a minimum.

3.1. Spectral Characteristics at Minimum

Walborn (1977) described the characteristics of a spectrum of HD 5980 obtained between 1973 and 1976 as follows: "broad He II 4686 emission with extensive wings; P Cygni profiles at N v $\lambda\lambda$4604, 4620; strong N IV $\lambda\lambda$3479-3483-3485 emission but no N IV λ4058. Well-marked He I absorption, but only traces of He II." HD 5980 was subsequently classified WN4+07I: by Breysacher et al. (1982) based on RV variations of He II 4686 and the presence of the O-type photospheric absorption lines in the spectrum. They associated the emission-line spectrum with star B, and assumed that the photospheric absorptions originated in star A. We now know that the photospheric absorptions visible in the spectra of Breysacher et al. (1982) and those in spectra obtained over the decade of the 1990s are quasi-stationary and arise in the third star of the system (Niemela 1988; Schweickhardt 2000; Koenigsberger et al. 2002; Foellmi et al. 2008), although this does not exclude the presence of photospheric absorptions arising in star A (or star B for that matter). Such lines have not yet been unambiguously identified in any of the spectra other than those obtained near eruption maximum (Koenigsberger et al. 1996), and these could simply have been produced in a pseudo-photosphere. We thus have no information regarding the photospheric properties of star A. On the other hand, we know that star A has displayed a WN-type emission line spectrum at least since the early 1980s, since Niemela (1988) measured RV variations of N v 4604, 4620 indicating their presence in this star. Subsequently, the N IV 4058 emission line has been shown to follow the motion of star A, as does the semi-forbidden N IV] 1486 line in all UV spectra where it is visible. Thus, there is little question that since $\sim$ 1980, star A's wind dominates the emission-line spectrum, which until recently has been that of a "late" WN-type star. The most recent optical spectrum obtained in 2009 August 29 indicates a spectral subtype around WN4/5, given the relative line intensities N IV 4058 > N v 4603 > N III 4640 Å. At this spectral type, HD 5980 is the first LBV to have such a hot temperature at minimum.

3.2. Is HD 5980 an S Doradus Variable?

S Doradus variables are hot luminous stars that undergo intrinsic photometric and/or spectroscopic variability on various timescales, including eruptions (van Genderen 2001; de Groot & Sterken 2001). S Dor-like variability is characterized by semi-periodic changes in spectral type and brightness which were originally interpreted as due to an ejection of a shell, but as

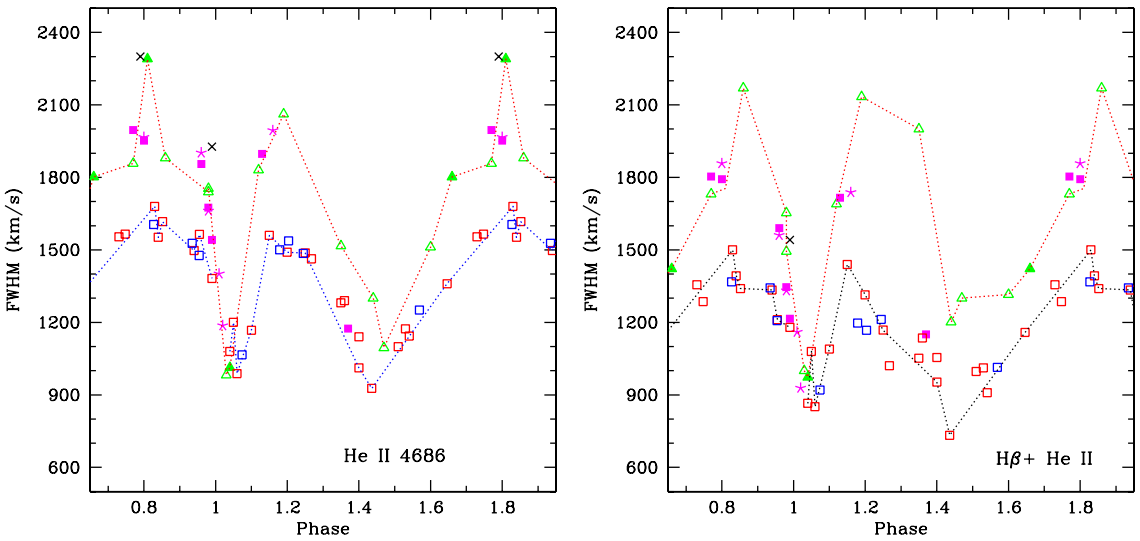

Figure 5. Plots of FWHM for He II 4686 (left) and Hβ+ He II (right). Symbols correspond to different epochs: 1955–1958 (filled-in triangle); 1959–1965 (open triangle); 1977 (cross); 1998–1999 (open square); 2005 (filled-in square); 2006 (star). Dashed lines connect the 1955–1965 and the 1999 data points illustrating that in both epochs the variability trends are the same, although the amplitudes differ.

(A color version of this figure is available in the online journal.)

shown by Leitherer et al. (1994) and Groh et al. (2009) for the case of AG Car, can only be understood in terms of a change in the stellar radius. In this context, Koenigsberger et al. (1998a) suggested that the changing wind speed observed in HD 5980 over the 1979–1995 timespan could potentially be associated with an increasing stellar radius. However, it remains to be shown that its spectrum and bolometric luminosity are indeed consistent with such a scenario. If the radius did indeed increase, then the two sudden eruptive events that occurred in 1993 and 1994 could have been triggered by the presence of the binary companion. Specifically, because tidal forces increase rapidly with increasing radius, a critical size $R_{\rm crit}$ is attained whereby the combined effect of radiation pressure and gravitational perturbations may lead to an enhanced stellar mass ejection. Thus, the large mass-loss rate deduced from the 1994 spectrum of HD 5980 (Koenigsberger et al. 1998b; Drissen et al. 2001) may correspond to this mass ejection phase.

An extended Hα emission surrounding HD 5980 is present in a recent *HST*/ACS WFC image of the NGC 346 cluster (R. Barbá 2010, in preparation). The presence of ejecta from the 1993–1994 eruptions was also inferred by Cellone et al. (1996) from a difference in the pre- and post-eruption polarization data, indicating the presence of additional circumbinary material in 1995, compared to 1987–1991.

Thus, we tentatively suggest that HD 5980 may be an S Dor variable in which the slow changes it has displayed occur as a consequence of a deep-seated, long-term variability pattern associated with a slowly increasing radius and that the brief and more violent eruptions were triggered by the binary companion.

4. ORBITAL PHASE-DEPENDENT VARIABILITY

Spectral variations in HD 5980 are well known to correlate with orbital phase. Perhaps the most distinguishing feature of this variability is the changing FWHM of its WR-type emission lines (Feast et al. 1960; Breysacher & Westerlund 1978)—the FWHM decreases by almost a factor of 2 around eclipse phases compared with phases around elongations (Breysacher et al. 1982; Moffat et al. 1998; Breysacher & Francois 2000).

Typical FWHM variations are illustrated in Figure 5 where the He II 4686 and Hβ+ He II FWHM are plotted as a function of the orbital phase, centered at $\phi = 0.0 = 1.0$. Although the variations are always the same from a qualitative standpoint, quantitative changes from epoch to epoch are observed. Consider, for example, He II 4686. At $\phi = 1.00$–1.06, FWHM $\sim$ 900–1000 km s^{-1} always, but at $\phi \sim 1.8$, FWHM $\geqslant$ 1900 km s^{-1} during 1955–1962 and 2005–2006, while in 1999, FWHM $\sim$ 1600 km s^{-1}.

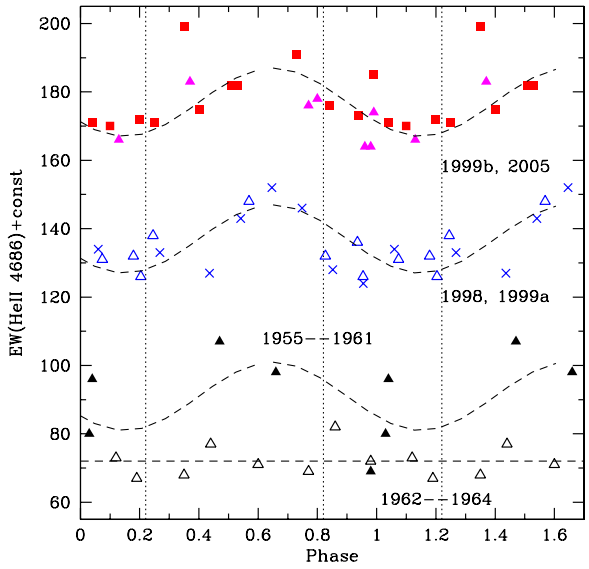

Figure 6. Plot of EW as a function of the orbital phase for different epochs in our data, as indicated. Vertical shifts are applied to epochs starting in 1998 for clarity. The epochs 1999a and 1999b refer to the early and latter parts of 1999, respectively. Dashed curves illustrate that most epochs exhibit the same phase-dependent trend. The dotted vertical lines indicate the orbital phases where FWHM is maximum. Eclipses are at $\phi = 0.0$ and 0.36. The EWs are not corrected for eclipse effects.

(A color version of this figure is available in the online journal.)

There is no general correlation between the FWHM variations and the overall strength of the He II4686 and Hβ+ He II emission lines, as characterized by their EW. The EW of He II 4686 is plotted in Figure 6 as a function of the orbital phase for the different epochs (separated by vertical shifts in the plot). The phase dependence is clearly different: the EWs are at a maximum

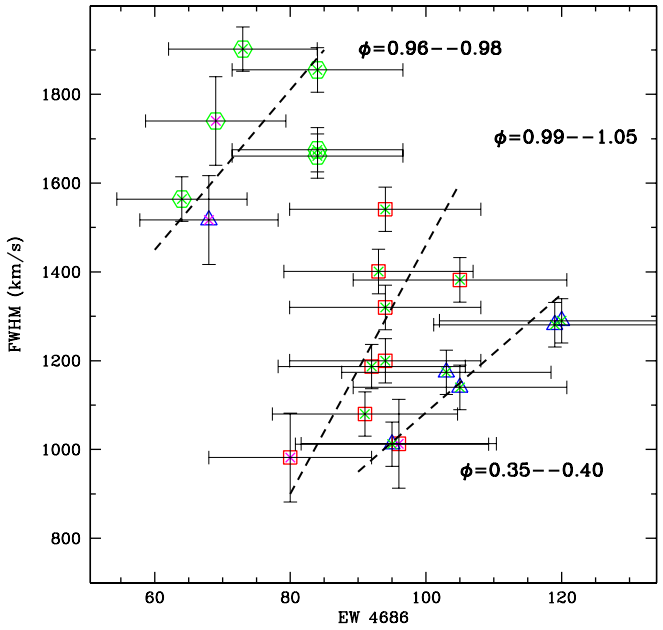

Figure 7. Possible correlation between FWHM and EW in the He II 4686 emission line for different epochs within three orbital phase bins: 0.35–0.40 (triangles), 0.99–1.05 (squares), and 0.96–0.98 (hexagons). Error bars indicate adopted 15% EW and 50 km s^{-1} uncertainties. The dashed lines indicate the general trends of the data within each phase bin.

(A color version of this figure is available in the online journal.)

near phase 0.65, while the FWHMs are maximum at $\phi \sim 0.2$ and 0.8. It is interesting to note that the epoch which does not show a clear EW modulation (1962–1964) also differs from the other epochs in that the average EW is significantly smaller. If the data of small phase bins are analyzed, however, a possible correlation between FWHM and EW emerges, for orbital phases near eclipses, as illustrated in Figure 7. The clearest case is the phase bin 0.35–0.40, where an increase in FWHM of 300 km s^{-1} is accompanied by an increase of 25 Å in EW. Similar trends are seen in the phase bins 0.99–1.05 and 0.96–0.98.

The FWHM variations within an orbital cycle are associated with striking emission line profile variations. Figure 8 shows the 1962 and 1999 He II 4686 emission lines at different orbital phases within the same 19 day orbital cycle. Around eclipses, the line becomes highly asymmetrical and seems to develop a stronger emission near line center. One could argue that the increased intensity at line center is simply a consequence of the normalization to the continuum level, uncorrected for eclipse effects. This is, indeed, true for $\phi = 0$ (when star A is in the foreground), but not for the opposite eclipse, as we illustrate in Figure 9 where the He II 4686 and Hβ+ He II lines in the 1999 *HST*/STIS spectra are plotted on an absolute (undereddened) flux scale. An illuminating fact is that the energy contained in the emission lines is the same, within the uncertainties, at orbital phases 0.36 and 0.85, both of which are greater than that at $\phi = 0.05$. Thus, the energy contained in the emission lines decreases when star A is in the foreground, which is consistent with the notion that star B is a WNE star and contributes toward the overall emission line strength.

Figure 10 displays the He II 4686 and Hβ+ He II RV measurements, obtained by fitting a single Gaussian to the emission-line. The dashed curves are the expected RVs for a 70+54 $M_{\odot}$ binary system. Foellmi et al. (2008) show that these curves are consistent with the RV variations obtained from deblending the N IV 4057 line in the same FEROS spectra analyzed here. The He II 4686 and Hβ+ He II are not consistent with these curves, even in the "historic" spectra. Hβ+ He II does follow the

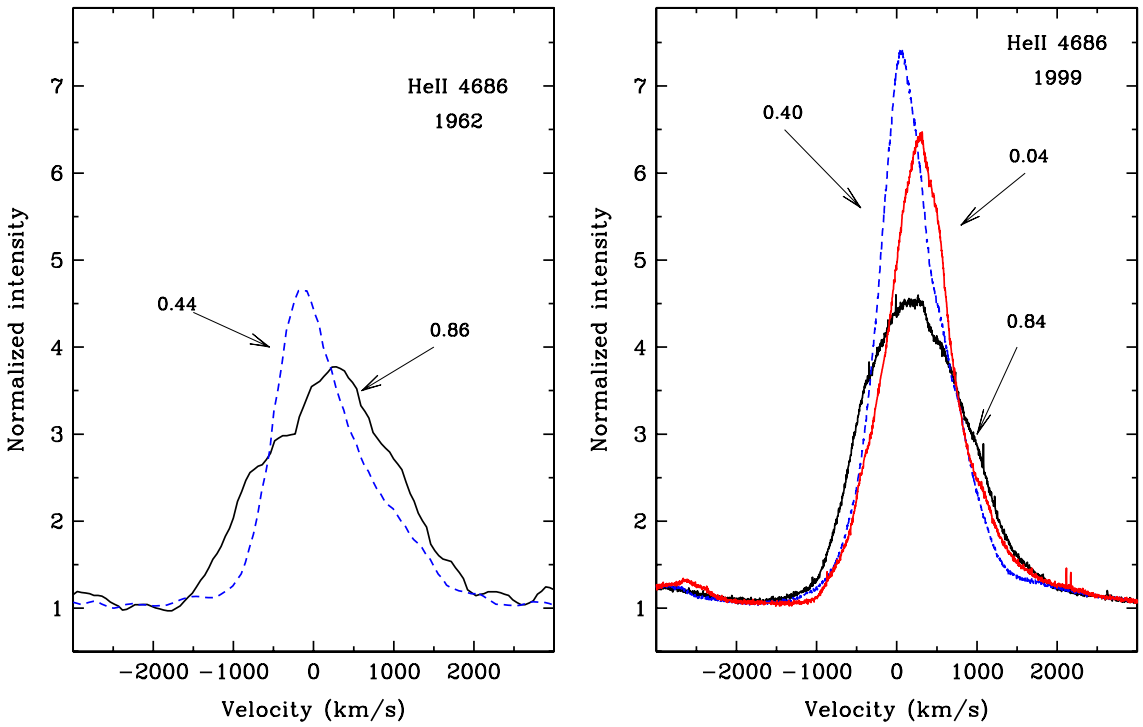

Figure 8. Montage of He II 4686 line profiles from a single orbital cycle normalized to the continuum level. Left: Radcliffe spectra of 1962. Right: FEROS spectra of 1999. Although the emission line strengths are significantly greater in 1999, the same orbital-phase-dependent line profile variability is observed during these two epochs.

(A color version of this figure is available in the online journal.)

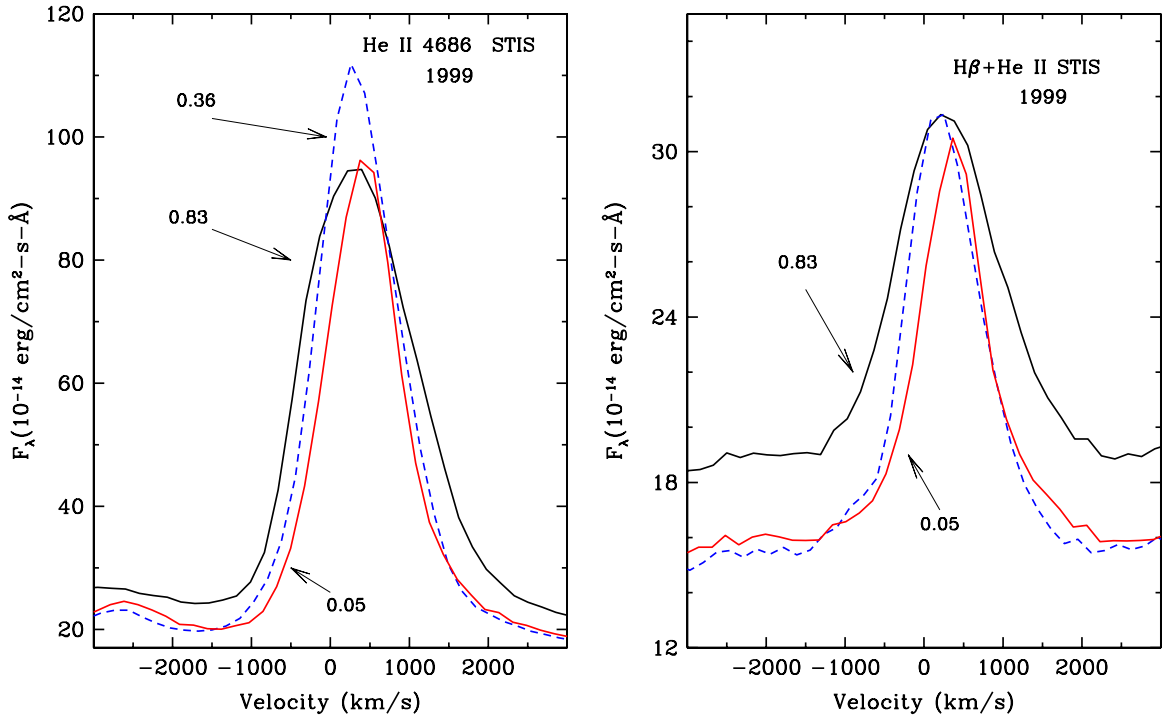

Figure 9. Montage of He II 4686 (left) and Hβ+ He II (right) profiles from a single orbital cycle of the 1999 *HST*/STIS observations, illustrating the line-profile variability on an absolute flux scale. The different continuum levels are due to the eclipses. Note that the central line intensity at $\phi = 0.36$ (dashes) is significantly stronger than expected if only eclipse effects are considered.

(A color version of this figure is available in the online journal.)

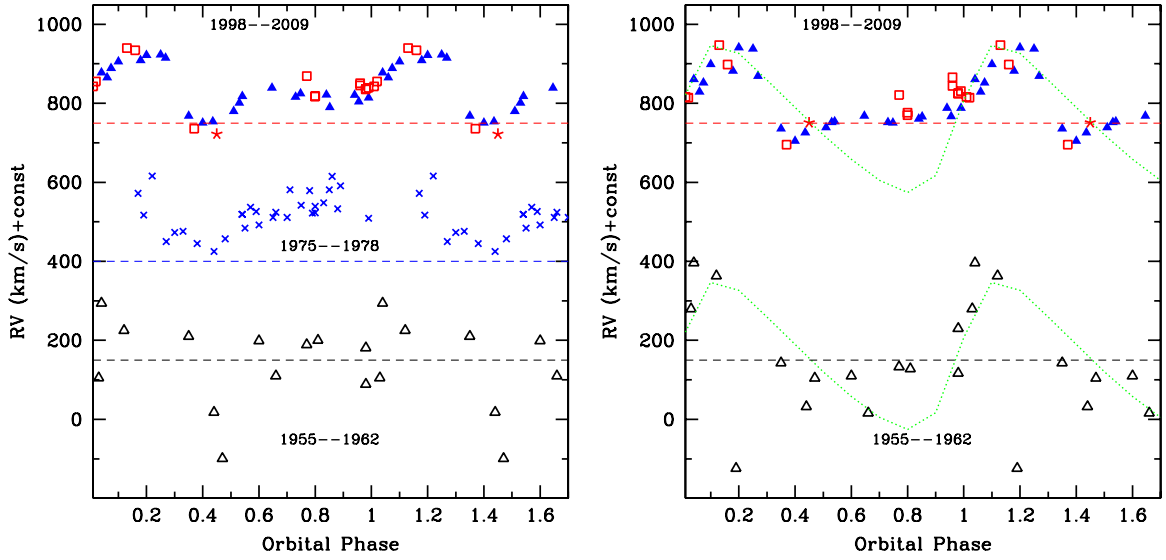

Figure 10. RV measurements of the emission lines using a single Gaussian fit. Left: He II 4686 from the Radcliffe spectra (bottom), from Breysacher et al. (1982) +250 km s^{-1} (middle), and recent epoch spectra + 600 km s^{-1} (top). The dashed lines correspond to the local SMC systemic velocity (assumed here to be +150 km s^{-1}), shifted by 0, +250, and +600 km s^{-1}. Different symbols used to represent the recent epochs are 1998–1999 (filled triangle); 2005–2005 (open square); 2009 (star). Right: corresponding Hβ+ He II measurements. The dotted curves correspond to the RV curve of star A obtained from N IV 4058 Å by Foellmi et al. (2008). Hβ+ He II tends to follow the orbital motion of this star during part of the orbital cycle only, with the largest discrepancies appearing in the phase interval 0.3–0.9.

(A color version of this figure is available in the online journal.)

expected orbital motion of star A between orbital phases 0 and 0.36, but at other phases, there is little or no correspondence. The remarkable thing about the Hβ+ He II behavior is that its RV measurements lead to a similar phase-dependent behavior regardless of epoch. This implies that the mechanism involved in producing the Hβ+ He II variations is not strongly dependent on the wind characteristics of the two stars. On the other hand, the trends of the He II 4686 RVs vary from epoch to epoch: the 1955–1965 data set shows no phase modulation, except for a "blue excursion" around $\phi = 0.4$ (see below); the 1975–1978 data of Breysacher et al. (1982) which we reproduce here, display maximum positive RVs around $\phi = 0.8$–1.0; while the 1998–2009 data display a maximum near $\phi = 0.2$, the latter consistent with the orbital motion of star A. Hence, the variability of He II 4686 does appear to depend on the stellar wind properties.

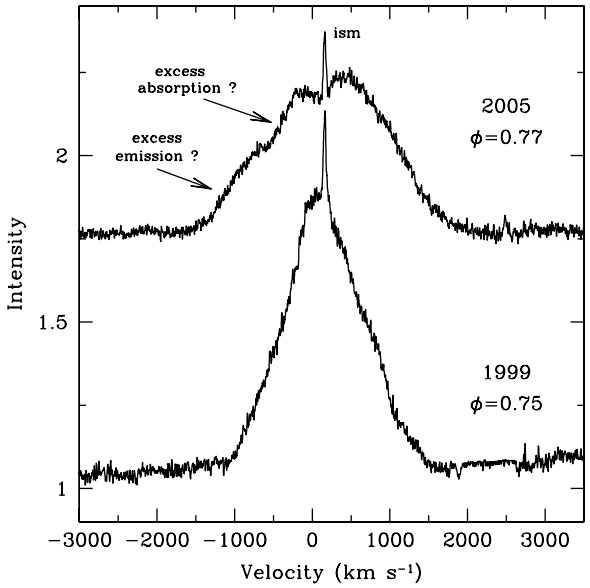

Figure 11. Example of the Hβ line profiles illustrating the source of uncertainty in the determination of an RV curve for the system. The extended and asymmetric wings may be interpreted as emission from the stellar winds of stars A and B, deformed by superposed absorption, or from the outflows associated with the wind–wind interaction regions. The sharp central emission arises in the N66 nebula.

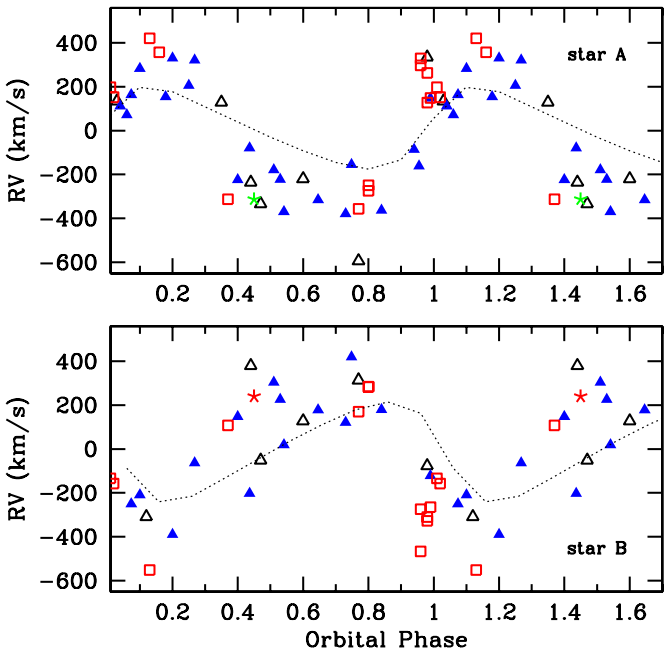

Figure 12. RV measurements of Hβ+ He II derived from fits performed using two Voigt line shapes. The derived RVs may be associated with orbital motion of star A (top) and star B (bottom), although their amplitude is significantly larger than that of the RV curves derived by Foellmi et al. (2008), shown as the dotted curves. Symbols are the same as in Figure 10. RV's are corrected for the SMC systemic motion.

(A color version of this figure is available in the online journal.)

As mentioned in Section 2.3, the use of a single Gaussian to describe the emission lines in HD 5980 is a gross simplification, and the RVs that are thus derived are simply a diagnostic of the epoch-dependent behavior of the emission-line profiles. Figure 11 shows why it is so difficult to derive a reliable RV curve from most of the emission lines in HD 5980. This figure is a plot of Hβ+ He II at two different epochs at nearly the same orbital phase, both showing similar asymmetries but with the wings in 2005 being more extended than in 1999. One can interpret these profiles in at least three ways. The first interpretation is that the depression near the top of the blue wing is an absorption feature that is superposed on the emission, with the absorption either being a broad photospheric line or a P Cygni absorption. The second interpretation is that there is excess emission near the base of the blue wing which could be produced, for example, in a wind–wind interaction region. The third interpretation is that the extended and asymmetric wings correspond to the contributions from the stellar winds of stars A and B and that the orbital motion leads to the line-profile variability. If the latter interpretation is adopted, then one may proceed to fit two functions to the line profiles. Figure 12 displays the result of deblending the Hβ+ He II emission line using two Voigt functions. It is interesting to note that the two RV curves are consistent with the RV curves derived by Foellmi et al. (2008) for N IV 4057 Å, although their amplitudes are significantly larger. We stress, however, that the sources of the line-profile variability must be understood before we may associate with orbital motion the RV variations derived from emission lines in HD 5980.

The "blue excursion" of the He II 4686 RVs around ϕ = 0.4–0.5 is a systematic effect (see also Breysacher et al. 1982) which we can see from Figure 13 is caused by a shift to shorter wavelengths of the maximum in the line emission around these phases.

In summary, we find that (1) the same type of line-profile, FWHM and EW variations over orbital phase persist over all observational epochs, despite changes in the line intensities from epoch to epoch; (2) Hβ+ He II displays RV variations that are similar from epoch-to-epoch, unlike He II 4686 which appears to depend on the epoch of observation; (3) the centroid measurements of Hβ+ He II indicate its presence primarily in star A, although a two-function fit to the line, if applicable, leads to the conclusion that both stars contribute significantly to this emission; (4) the systematic departure from the Foellmi et al. (2008) RV curve observed in the orbital phase interval 0.4–0.5 is produced by the appearance of an additional blueshifted emission component around this phase interval.

From a purely phenomenological standpoint, there are two intriguing aspects of the periodic line-profile variations: (1) to our knowledge, no other binary system undergoes such large systematic variations, although numerous WR binary systems do exist; and (2) it is persistently found in HD 5980 spectra, despite the strong epoch-to-epoch variability in their strength and continuum brightness. The FWHM variability has been interpreted in terms of wind–wind collisions (Moffat et al. 1998; Breysacher & Francois 2000). Koenigsberger (2004) argued that the wind eclipses would also be expected to make emission lines narrower because the additional P Cygni absorption "eats away" at both the blue and red emission wings when the line is formed inside the orbital radius (Auer & Koenigsberger 1994; Koenigsberger et al. 2006). In addition, the irradiation of the sub-binary hemisphere by the companion can either inhibit the stellar wind from attaining maximum expansion speed (Stevens & Pollock 1994) or produce a sudden "radiative braking" effect (Gayley et al. 1997). A more unconventional scenario involves actual changes in the intrinsic wind structure, possibly driven by the varying tidal force over the binary orbit (Koenigsberger & Moreno 1997; Koenigsberger et al. 2010). All of these physical processes are expected to be present in HD 5980 to some degree

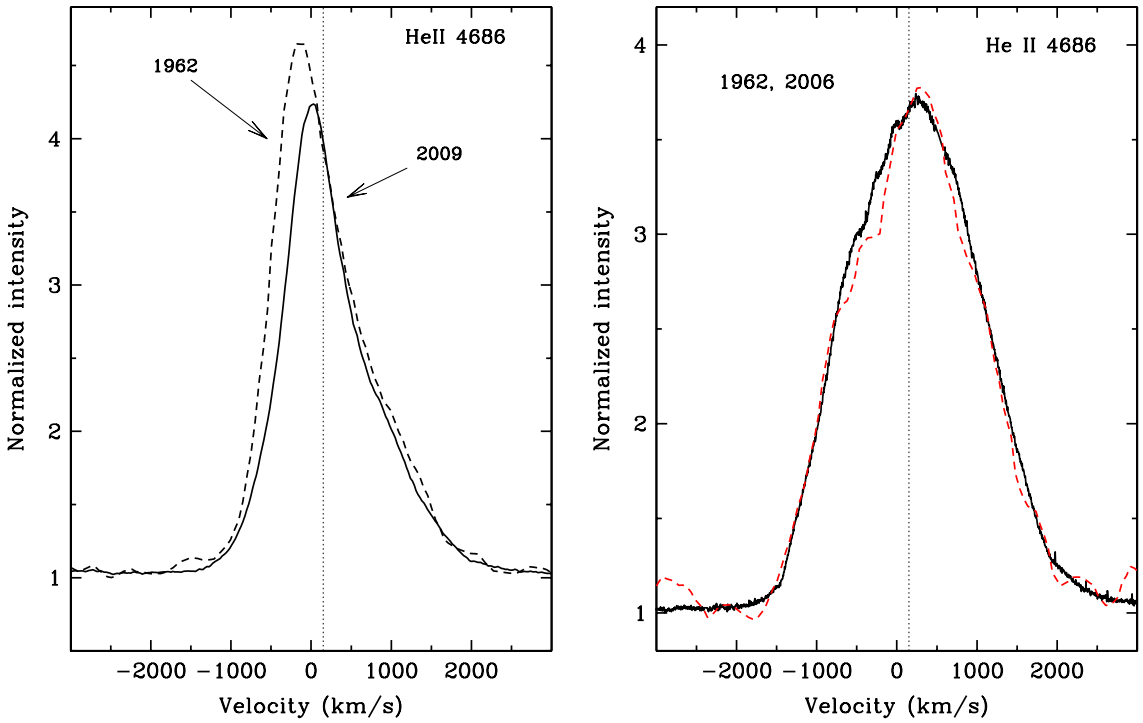

Figure 13. Comparison of He II 4686 line profiles in 1962 and recent observations. Left: orbital phase around 0.4, showing the excess blue emission that causes the "blue excursion" in the RV curves. Right: orbital phase around 0.8, showing the more symmetric Gaussian-like line profile. The vertical dotted line in each panel shows the adopted systemic SMC velocity +150 km s^{-1}.

(A color version of this figure is available in the online journal.)

or other, but it will require a detailed modeling effort in order to determine their relative importance.

5. CONCLUSIONS

In this paper, we analyzed spectroscopic data obtained over more than five decades which show that the strong emission-line state of HD 5980 that started during the early 1980s is ending, with an expected minimum to occur within the next few years. This long "high" state peaked sometime between the years 1994 and 2000. The brief and violent eruptions of 1993 and 1994 occurred at the start of a prolonged maximum state of activity. We also find evidence indicating that an earlier "high" state may have occurred between 1960 and 1965, thus suggesting the possibility that the long-term variability may be cyclical on a $\sim$ 40 year timescale. This long-term, possibly cyclic variability is similar to that which is observed in LBVs such as η Car and AG Car. There are other similarities between HD 5980 and LBVs. (1) Its spectrum changed from WN7-11 near maximum in the eruption visual light curve to WNE near minimum, which implies cooler effective temperature during the most active state. (2) Observational evidence supports the presence of ejecta associated with the 1993, 1994 eruptions (R. Barbá 2010, in preparation; Cellone et al. 1996). On the other hand, there are two characteristics that make HD 5980 an outstanding member of the LBV class. First, it is a close binary system. The only other known LBV binary, η Car (Damineli et al. 2008), has a very long orbital period ($\sim$ 5.5 years). Second, its effective temperature during maximum is significantly hotter than any of the other known LBVs. HD 5980's lowest temperatures appear to have been in the vicinity of those of early B-type stars, while most LBVs exhibit A-type spectra during maximum in the visual light curve. We note that this second characteristic may be related to the first. That is, the binary interaction effects may have facilitated the ejection of the outer layer that would ordinarily constitute the very extended, cooler envelope associated with the LBV maximum. In other words, if HD 5980 were not a close binary system, its effective temperature may have become significantly cooler than early B-type, and it might have remained as such during more than a decade. If this is indeed the case, then HD 5980 provides the unique opportunity of viewing deeper, otherwise unseen layers of an LBV during the maximum in its activity cycle.

Given the above, the importance of clearly understanding the causes and the effects produced by binary interactions is highlighted. The set of photographic spectra from the Radcliffe Observatory that we digitized indicates that the strong emission line profile variability generally observed over the 19 day orbital period was also present during the 1955–1965 decade. The persistence of these effects, despite changes in the stellar wind characteristics of the system, indicates that they are related to a process governed more by the orbital phase than by the properties of the stellar winds. The detailed analysis of the binary interaction effects will surely yield further insight into the physical properties of this system.

We thank Tom Lloyd Evans, Michael Feast, and David Kilkenny for making the Radcliffe Telescope plates available to us; Nolan Walborn for data from 1973 and 1977 and Phil Massey for data from the early 1980s; and Jura Borissova and NAO "Rozhen" for allowing us the use of the densitometer. This paper makes use of data gathered with the 6.5 m Magellan telescopes located at Las Campanas Observatory, Chile. The *Hubble Space Telescope* is operated by the Space Telescope Science Institute, under contract with the Association of Universities for Research in Astronomy. G.K. and L.G. acknowledge support from UNAM/DGAPA/PAPIIT grants IN106708, IN123309, and CONACYT grant 48929. R.H.B. acknowledges partial support

from ULS DIULS grant, and D.J.H. acknowledges support from grant HST-GO-11623.01-A.

REFERENCES

Auer, L. H., & Koenigsberger, G. 1994, ApJ, 436, 859
Azzopardi, A., & Vigneau, J. 1975, A&AS, 22, 285
Barbá, R. H., Niemela, V. S., Baume, G., & Vázquez, R. A. 1995, ApJ, 446, L23
Barbá, R. H., Niemela, V. S., & Morrell, N. I. 1997, in ASP Conf. Ser. 120, Luminous Blue Variables: Massive Stars in Transition, ed. A. Nota & H. Larmers (San Francisco, CA: ASP), 238
Barbá, R. H., et al. 1996, RevMexAA Conf. Ser., 5, 85
Bateson, F. M., & Jones, A. 1994, Publ. Var. Star. Sec. R. Astron. Soc. New Zealand, 19, 50
Breysacher, J., & Francois, P. 2000, A&A, 361, 231
Breysacher, J., Moffat, A. F. J., & Niemela, V. 1982, ApJ, 257, 116
Breysacher, J., & Perrier, C. 1980, A&A, 90, 207
Breysacher, J., & Perrier, C. 1991, in IAU Symp. 143, Wolf–Rayet Stars and Interrelations with other Massive Stars in Galaxies, ed. K. van der Hucht & B. Hidayat (Dordrecht: Kluwer), 229
Breysacher, J., & Westerlund, B. E. 1978, A&A, 67, 261
Cellone, S. A., et al. 1996, RevMexAA Conf. Ser., 5, 123
Crowther, P. 2006, in ASP Conf. Ser. 353, Stellar Evolution at Low Metallicity: Mass Loss, Explosions, Cosmology, ed. H. Lamers et al. (San Francisco: ASP), 157
Damineli, A., et al. 2008, MNRAS, 384, 1649
de Vaucouleurs, G. 1968, Appl. Opt., 7, 1513
de Groot, M., & Sterken, C. (ed.) 2001, in ASP Conf. Proc. 233, P Cygni 2000: 400 Years of Progress (San Francisco, CA: ASP)
Drissen, L., Crowther, P. A., Smith, L. J., Robert, C., Roy, J.-R., & Hillier, D. J. 2001, ApJ, 545, 484
Feast, M. W., Thackeray, A. D., & Wesselink, A. J. 1960, MNRAS, 121, 337
Foellmi, C., et al. 2008, RevMexAA, 44, 3
Gayley, K. G., Owocki, S. P., & Cranmer, S. R. 1997, ApJ, 475, 786
Groh, J. H., Hillier, D. J., Damineli, A., Whitelock, P. A., Marang, F., & Rossi, C. 2009, ApJ, 698, 1698
Hamann, W.-R., Koesterke, L., & Wessolowski, U. 1993, A&A, 274, 397
Heydari-Malayeri, M., Courbin, F., Raauw, G., Esslinger, O., & Magain, P. 1997, A&A, 326, 143
Kaufer, A., Schmid, H. M., Schweickhardt, J., & Tubbesing, S. 2002, in ASP Conf. Ser. 260, Interacting Winds from Massive Stars, ed. A. F. J. Moffat & N. St-Louis (San Francisco, CA: ASP), 489
Kimble, R. A., et al. 1998, Proc. SPIE, 3356, 188
Koenigsberger, B., Shore, S. S., Guinan, E., & Auer, L. H. 1996, RevMexAA Conf. Ser., 5, 92
Koenigsberger, G. 2004, RevMexAA, 40, 107
Koenigsberger, G., Auer, L. H., Georgiev, L., & Guinan, E. 1998a, ApJ, 496, 934
Koenigsberger, G., Fullerton, A., Massa, D., & Auer, L. H. 2006, AJ, 132, 1527
Koenigsberger, G., Georgiev, L., Barbá, R., Tzvetanov, Z., Walborn, N. R., Niemela, V., Morrell, N., & y Schulte-Ladbeck, R. 2000, ApJ, 542, 428
Koenigsberger, G., Guinan, E., Auer, L. H., & Georgiev, L. 1995, ApJ, 452, L107
Koenigsberger, G., Kurucz, R., & Georgiev, L. 2002, ApJ, 581, 598
Koenigsberger, G., & Moreno, E. 1997, in ASP Conf. Ser. 120, Luminous Blue Variables: Massive Stars in Transition, ed. A. Nota & H. Lamers (San Francisco, CA: ASP), 233
Koenigsberger, G., Peña, M., Schmutz, W., & Ayala, S. 1998b, ApJ, 499, 889
Koenigsberger, G., et al. 1994, ApJ, 436, 301
Koenigsberger, G., et al. 2001, AJ, 121, 267
Koenigsberger, G., et al. 2009, in ASP Conf. Ser. 425, Hot and Cool: Bridging Gaps in Massive Star Evolution, ed. C. Leitherer et al. (San Francisco, CA: ASP), in press
Leitherer, C., et al. 1994, ApJ, 428, 282
Massey, P., & Duffy, A. S. 2001, ApJ, 550, 713
Mendoza, E. E. 1970, Bol. Obs. Tonanzintla Tacubaya, 5, 269
Moffat, A. F. J., et al. 1998, ApJ, 497, 896
Niemela, V. S. 1988, in ASP Conf. Ser. 1, Progress and Opportunities in Southern Hemisphere Optical Astronomy, The CTIO 25th Anniversary Symposium, ed. V. M. Blanco & M. M. Phillips (San Francisco, CA: ASP), 381
Niemela, V. S., Barbá, R. H., Morrell, N. I., & Corti, M. 1997, in ASP Conf. Ser. 120, Luminous Blue Variables: Massive Stars in Transition, ed. A. Nota & H. J. G. L. M. Lamers (San Francisco, CA: ASP), 222
Perrier, C., Breysacher, J., & Rauw, G. 2009, A&A, 503, 963
Pojmanski, G. 2002, Acta Astron., 52, 397
Schweickhardt, J. 2000, PhD thesis, Ruprecht-Karls-Universität, Heidelberg
Sterken, C., & Breysacher, J. 1997, A&A, 328, 269
Stevens, I. R., & Pollock, A. M. T. 1994, MNRAS, 269, 226
van den Bergh, S. 1976, IAU Circ., 2993, 2
van Genderen, A. M. 2001, A&A, 366, 508
Villar-Sbaffi, A., Moffat, A. F. J., & St.-Louis, N. 2003, ApJ, 590, 483
Walborn, N. R. 1977, ApJ, 215, 53